

Mechanical properties of CNT reinforced hybrid functionally graded materials for bioimplants

M. Asif HUSSAIN¹, Adnan MAQBOOL^{1,2}, F. Ahmad KHALID¹, Nabi BAKHSH¹, Ali HUSSAIN²,
Jamil Ur RAHMAN², Jong Kyu PARK², Tae Gone PARK², Lee Jae HYUN², Myong Ho KIM²

1. Faculty of Materials Science and Engineering, GIK Institute of Engineering Sciences and Technology,
Topi, KPK, Pakistan;

2. Engineering Research Center for Integrated Mechatronics Materials and Components,
Changwon National University, Gyeongnam 641-773, Korea

Received 18 June 2013; accepted 18 November 2013

Abstract: The hybrid functionally graded materials (FGM) of hydroxyapatite (HA), stainless steel 316L (SS316L) and carbon nanotubes (CNT) were synthesized for biomedical implants. Three different types of FGM were produced by the combination of SS316L and CNT to reinforce HA in discrete layers of FGM. In the first type of FGM, concentration of SS316L was varied from 10% to 40% (mass fraction) with an increment of 10% to reinforce micro HA. In the second type of FGM, 0.5% (mass fraction) functionalized CNT was added by maintaining the rest of composition as that of the first type of FGM. In the third type of FGM, mixture of micro and nano HA (mass ratio 1:1) was used, keeping rest of composition similar to the second type of FGM. All types of FGM were subjected to uniaxial compaction and sintered by pressureless sintering technique at similar compaction and sintering parameters. The results show that the densification is enhanced with the addition of CNT and nanocrystalline HA in the FGM. Hardness and fracture toughness increase in both FGM reinforced with CNT, but the increase of the hardness and fracture toughness are more pronounced in FGM with micro and nanocrystalline HA.

Key words: functionally graded materials; hydroxyapatite; nanocomposites; biomaterial; implant

1 Introduction

There is a continuous demand for materials with good biomedical and mechanical properties that can be used for biomedical implants. Hydroxyapatite (HA, $\text{Ca}_{10}(\text{PO}_4)_6(\text{OH})_2$) has been investigated intensively for the replacement and repair of teeth and bones because of its similar chemical composition to the natural apatite and biocompatibility with not only hard tissues but also muscle and skin tissues and it bonds directly to the bones without cytotoxic effects [1–3]. Unfortunately, HA bears poor mechanical properties as compared to bone, which limits its use in major load bearing applications [4]. On the other hand, stainless steel 316L (SS316L) has been employed for a long time for implantation applications due to their excellent mechanical and corrosion resistant properties [5–7]. However, some studies have shown that SS316L is prone to crevice and pitting corrosion and induces cell toxicity by releasing Cr and Ni ions in the

human body [8–10]. To avoid the direct contact of metallic implants with the bones and tissues, biocompatible HA coatings have been employed on SS316L prosthesis [11]. However, the long term stability of these coatings is of concern because HA deposited coatings on metallic implant deteriorates due to poor interface bonding between metal and ceramic, resulting in failure of the surgery [12,13]. The concept of functionally graded materials (FGM) can be utilized to overcome these issues. The dissemination of two different materials in FGM will be beneficial in eliminating the direct macroscopic contact of these two materials with the bones and tissues in the joints. Mechanical and biological properties of HA have also been improved by introducing carbon nanotubes (CNT). In their studies, XU et al [14] and BALANI et al [15] have shown that addition of CNT not only improves the mechanical properties of HA, but also enhances its bioactivity.

In this work hybrid functionally graded materials of

HA, SS316L and CNT were fabricated by the pressureless sintering technique to fabricate the FGM by the powder metallurgy process and characterize their physical and mechanical properties by different techniques.

2 Experimental

Hydroxyapatite powders of average particle sizes of 5 μm and 40 nm (Ensail Co. Ltd, China), SS316L powder of average particle size of 8 μm (Sandvik Osprey Ltd, England) and CNT of average diameter of 13 nm (Sun Nanotech Co. Ltd, China) were used in the present study. HA and SS316L powders were used in the as-received form while CNTs were acid treated before mixing with HA. CNTs were first purified with concentrated solution of HCl to remove impurities like amorphous carbon, nanocrystalline graphite, and transition metal catalyst particles. After purification, CNTs were functionalized by treating them with concentrated solution of HNO_3 and H_2SO_4 in a volume ratio of 1:3. Three different sets of compositions were made to fabricate the FGM as shown in Table 1. In all three sets of FGM, concentration of SS316L was graded from 10% to 40% (mass fraction). The powders for different compositions were mixed by using planetary ball mill (Retsch PM-400) for 12 h in ethanol followed by drying to remove the ethanol. The layers of FGM were stacked manually in the die according to the scheme shown in Table 1 and pressed uniaxially at 150 MPa to make green compacts having diameter and height of 10 mm and 4.5 mm respectively. PVA was added to enhance the bonding between the powder particles and FGM layers. Composite compacts of each layer of FGM were also prepared under the same conditions.

Green compacts were sintered at 950 $^\circ\text{C}$ in the vacuum of 1 MPa for 3 h. In the sintering cycle, three dwells of 30 min were provided. Remaining liquid (i.e. water and ethanol) was evaporated during first dwell at 120 $^\circ\text{C}$. The second and third dwells at 300 $^\circ\text{C}$ and 550 $^\circ\text{C}$ were provided to escape the decomposed gases

from the sintering compacts. In the whole sintering process, heating and cooling rates were kept at 2 $^\circ\text{C}/\text{min}$ and 3 $^\circ\text{C}/\text{min}$, respectively.

Relative densities of FGM were calculated by measuring the sintered density of FGM in distilled water by Archimedes' principle and dividing it with theoretical density of FGM. Theoretical densities of FGM were calculated by using rule of mixtures. Different phases presented in the sintered body were identified by the X-ray diffraction (XRD). For microstructural evaluations, samples were cut in cross-sectional direction and then ground and polished. FGM of different compositions was examined by optical and scanning electron microscopy to observe the surface morphologies. Hardness of each layer (thickness $t=1$ mm) of FGM was measured by Vickers microindenter on the polished surfaces at a load of 1.96 N (200 g) for 15 s. Fracture toughness values of the first and fifth layer of each FGM was calculated by indentation method, utilizing a Vickers indenter at a load of 196 N (20 kg) for 10 s.

3 Results and discussion

3.1 Synthesis of FGM

FGM of HA-SS316L-CNT had been fabricated by the pressureless sintering technique. There was a compositional and microstructural gradient in the discrete layers of FGM, therefore thermal stresses may be produced by the different thermal expansion coefficients of the constituents of FGM during the fabrication process. To avoid the thermal stresses in the FGM, heating and cooling rates were kept low, therefore no cracks were observed within the layers or between the layers.

3.2 Powders morphology

Hydroxyapatite and SS316L were used in the as-received form. Before using these powders for the fabrication of FGM, SEM analyses were carried out to see the particles size distribution and morphology.

Figure 1(a) shows micro HA particles. Their shape

Table 1 Compositional variation of HA, SS316L and CNT in each layer of various FGM

Layer	Sample A	Sample B	Sample C
First	Micro HA	Micro HA+0.5%CNT	(50% micro/50% nano) HA+ 0.5% CNT
Second	Micro HA+10% SS316L	Micro HA+0.5% CNT+ 10% SS316L	(50% micro/50% nano) HA+ 0.5% CNT + 10% SS316L
Third	Micro HA+20% SS316L	Micro HA+0.5% CNT+ 20% S316L	(50% micro/50% nano) HA+ 0.5% CNT + 20% SS316L
Forth	Micro HA+30% SS316L	Micro HA+0.5% CNT+ 30% SS316L	(50% micro/50% nano) HA+ 0.5% CNT + 30% SS316L
Fifth	Micro HA+40% SS316L	Micro HA+0.5% CNT+ 40% SS316L	(50% micro/50% nano) HA+ 0.5% CNT + 40% SS316L

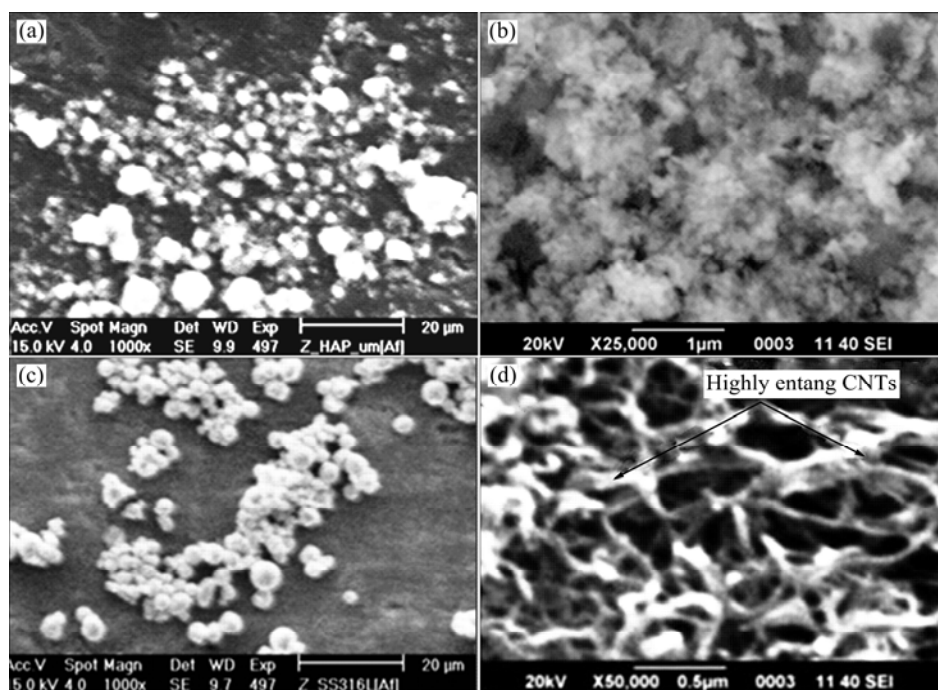


Fig. 1 SEM images: (a) Spherical particles of micron size HA; (b) Nanocrystalline HA particles appeared to be agglomerated; (c) SS316L revealing spherical morphology of particles; (d) CNT showing very high entanglement and agglomeration

appears to be spherical and particles are well separated from each other. In Fig. 1(b) nano HA particles are shown. Here particles appear to be agglomerated and hence the establishment of shape and distribution is difficult to be ascertained.

SS316L particles are shown in Fig. 1(c). This figure shows that particles are spherical and separated from each other, showing no agglomeration. SEM analysis results revealed that particle size distribution of SS316L and micro HA were very close, and expected to bond well with each other during compaction and hence would result in good diffusion of particles and densification of FGM after sintering. CNTs were treated with acids to remove the impurities and decorate its surface with the functionalized groups. The morphology of CNT is shown in Fig. 1(d). It can be observed that as-received CNTs are highly entangled with each other and impurity particles are present on the surface of CNT. After acid treatment these impurities were removed and CNTs were functionalized with different groups on their surface.

3.3 Densification

In this work, different compositions of FGM were synthesized by pressureless sintering technique to study the effect of nano HA with micro HA and the incorporation of CNT on densification of FGM. The compositional variation of 10%SS316L was employed in different layers of FGM as reinforcing agent for HA. Three compositions of FGM, i.e. samples A, B and C, were selected as shown in Table 1.

Understanding the sintering behavior of different FGM is important as this allows designing objects with controlled grain growth, microstructure and mechanical properties. For better densification of different layers of FGM, it is necessary to use a densification agent. Therefore, PVA solution was used as densification agent. Sintering temperature and atmosphere play a critical role in the decomposition of HA. It was studied by SRIDHAR [11] that at 900 °C in vacuum of 1.333 MPa, there was no adverse effect of temperature on the sintering of HA coated SS316L samples. He reported that no phase transformation took place during the sintering of HA coated SS316L samples at 900 °C and below. WANG and CHAKI [16] also reported that due to decomposition of the HA, reduced densification was achieved at temperature higher than 1000 °C in vacuum and 1300 °C in air.

It is worth mentioning that when HA decomposes, densification is reduced, which will result in deterioration in mechanical properties [17]. Also in-vitro dissolution is enhanced due to decomposition of HA and other phases of calcium phosphate which are formed during sintering process [11]. Therefore, sintering was carried out at 950 °C in the vacuum to avoid the decomposition of HA.

From Fig. 2 it is clear that densification of FGM increases as CNT and nano HA were introduced in different FGM. In the first composition micro HA without CNT was used for sample A; very low value of densification for each layer was obtained and it increased

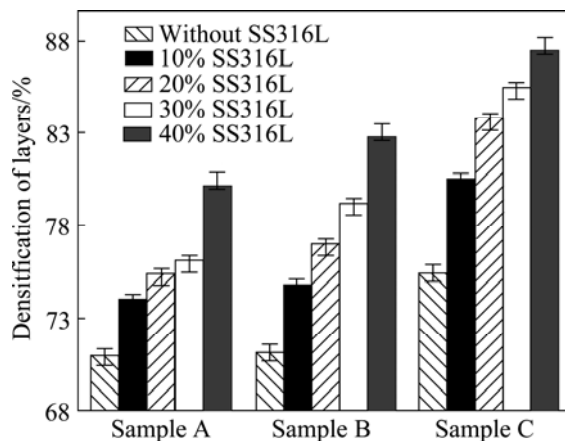


Fig. 2 Effect of different compositions on densification of FGM

with the addition of 0.5%CNTs with micro HA in the case of sample B. The reason is that CNTs are very small in size and can fill the pores between the particles in composite because they reside at the grain boundaries of HA particles. Therefore, densification of FGM was enhanced and porosity was reduced. This proves that CNT improves densification which will result in enhancement of the mechanical properties of FGM also.

In sample C where 50% nanocrystalline HA and 0.5% CNT had been employed with micro HA in all layers, densification was increased. The phenomenon of increasing densification in this case can be explained with the help of bi-modal mixtures of powders. Since this is bimodal/trimodal powders mixture, HA particles

with small diameter filled the pores between the large particles and enhance the sintering density. For a mixture having wide range of particle distribution, the maximum sintering density is obtained when large particles constitute a close packing and the remaining residual volume between the large particles is occupied by smaller particles. This occurs especially during the fast heating and large particles size distribution in the composite [18].

Therefore, in the present case, heating and cooling rates were kept low to avoid the cracking in the FGM. The particle size distribution between SS316L and micro HA was very close to each other which also avoided the cracking in FGM. It is clear that higher densification values were obtained in the case of sample B compared with sample A (i.e. 80% for monolithic micro HA layer and 82% for micro HA with CNT layer). Even higher values (i.e. 87.5%) were obtained in the case of sample C having nanocrystalline HA and CNT. This is because nanocrystalline HA and CNT filled the pores between these particles, improving the densification of this FGM layers as compared to sample A and sample B.

3.4 Microstructure

Each sample of FGM produced has five different and distinct layers. After sintering, disk-shaped samples were cut and ground with emery paper (4000 grit size) to study the cross-sectional view of different layers of these FGM. Distribution of SS316L particles in HA matrix in

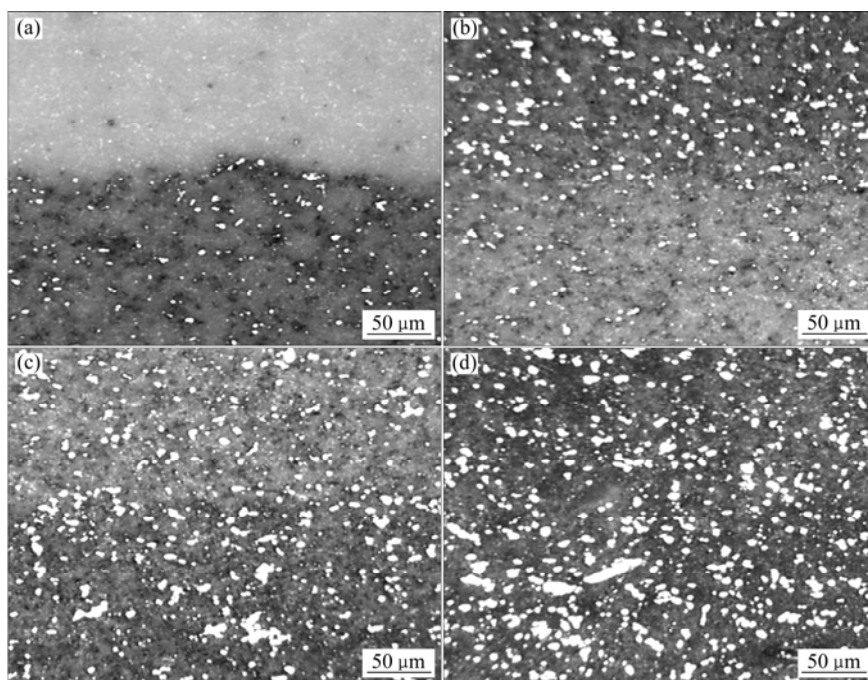


Fig. 3 Micrographs of sample A showing gradient of SS316L in HA (white area is SS316L in gray HA): (a) First layer and second layer; (b) Second layer and third layer; (c) Third layer and fourth layer; (d) Fourth layer and fifth layer

each layer of sample A is shown in Fig. 3. It is clear from Fig. 3 that particles of SS316L are dispersed evenly in HA matrix and very little agglomeration of SS316L is observed in the layers of FGM. CNTs were used in sample B and nanocrystalline HA in sample C with micro HA and SS316L in all layers of these FGM which is the only difference from sample A, therefore, surface morphology of these FGM is same as that of sample A under the optical microscope. It is observed that the bonding between layers is good and no cracks are observed around the boundary areas of the layers. However, manual stacking of layers in the die resulted in the non-uniform boundaries between the layers.

Figure 3 shows the different layers of sample A, revealing the distribution of SS316L particles in the matrix of HA. White area in each layer shows the SS316L particles in the grayish HA matrix. The first layer composed of monolithic HA, therefore white particles are absent here. With the increase of SS316L contents from 10% to 40% in the matrix of HA, white area in the layers is increased. Note that no cracks or defects generated in the layers during sintering. Distribution of SS316L particles is homogeneous in the matrix of HA; however, some agglomerated particles of SS316L are also observed in few areas of the layers. This may be due to the wet mixing process, used in the present work. In the micrograph it is clearly visible that SS316L particles are not deformed after the mixing and compaction process.

SEM analysis was done to assess the structural

features of the sintered FGM. Prior to SEM analysis a thin layer of gold was sputtered on the surface of the samples after grinding process to make a conductive path for the electrons. In order to observe the dispersion of CNT and other phases presented in different FGM in more detail, two layers (first & fifth layer) of sample B were examined.

The first layer (micro HA + 0.5% CNT) and fifth layer (micro HA + 0.5% CNT + 40% SS316L) of sample B are shown in Fig. 4(a) and Fig. 4(b) respectively. In Fig. 4, it is clear that CNTs are homogeneously dispersed and are present at the grain boundaries of HA and also embedded in the particles of HA.

In the case of ceramics based composites, it is difficult to get the clear view of presence of CNT, therefore, fractured samples were also observed under SEM. Figures 4(c) and (d) show the fractured surfaces of the first and fifth layer of sample B. In these figures, some embedded CNTs are pulled out and can be seen clearly. These CNTs reinforce the HA matrix and hence improve the mechanical properties of FGM ultimately.

3.5 Phase analysis

A Philips X-rays diffractometer with source of Cu K_{α} was used to identify the different phases presented and purity level of the final product. XRD spectra for the first and fifth layer of each FGM were taken to analyze the phases present in these layers after sintering at 950 °C in vacuum. Figures 5(a) and (b) show the spectra of the first and fifth layers of sample A which contains

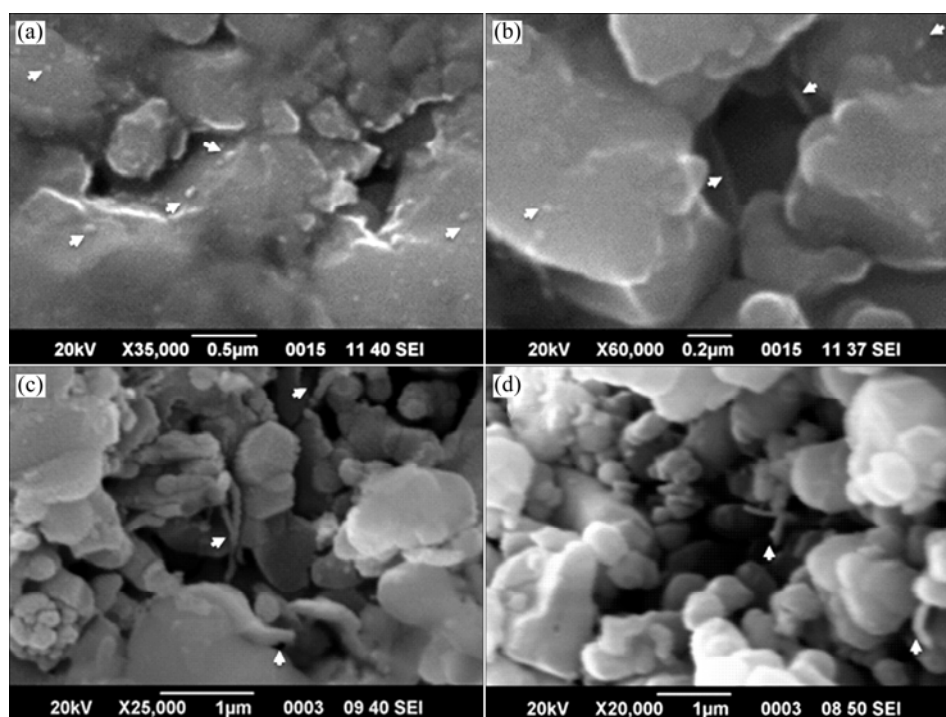


Fig. 4 SEM images of first layer and fifth layer of sample B: (a), (c) First layer; (b), (d) Fifth layer (CNTs are pulled out and also embedded; CNTs are presented in HA matrix as indicated by the arrows)

monolithic micro HA and micro HA + 40% SS316L respectively. Comparing Fig. 5(a) with standard spectrum of HA, it is confirmed that no other phase is present after sintering at 950°C in vacuum. Figure 5(b) shows the spectrum of the fifth layer of sample A which contains micro HA + 40% SS316L. It is intended from Fig. 5(b) that no phase transformation takes place. However, peak of HA at 2θ of -50.50° is superimposed by the peak of SS316L at the same position, therefore a very little peak broadening is observed at this point. WANG and CHAKI et al [16] studied the sintering behavior of HA under different atmospheres and temperatures. Their results showed that no phase transformation would occur if HA was sintered below 1000 °C in vacuum. SRIDHAR [11] studied the SS316L plates coated with HA and sintered at 900 °C in vacuum. Their results showed similar XRD spectrum as shown in the present study which shows that sintering has been done successfully without phase transformation.

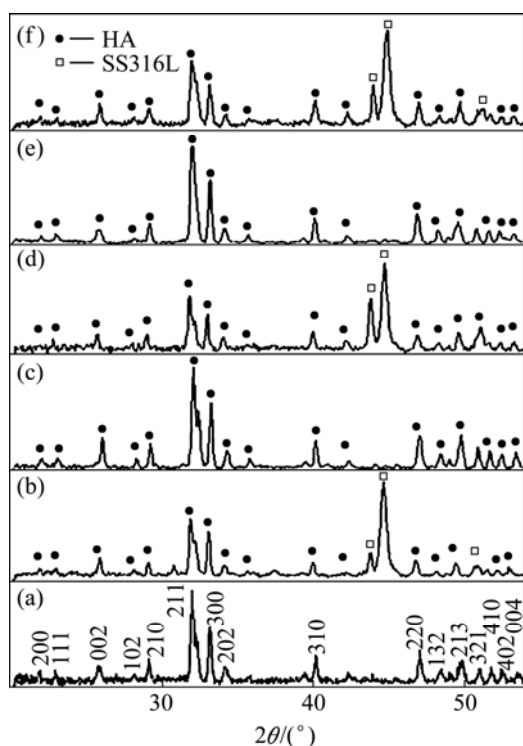


Fig. 5 XRD patterns of first and fifth layers of sample A, sample B and sample C: (a) Micro HA; (b) Micro HA + 40% SS316L; (c) Micro HA + 0.5% CNT; (d) Micro HA + 0.5% CNNT + 40% SS316L; (e) (50% micro/50% nano) HA + 0.5% CNT; (f) (50% micro/50% nano) HA + 0.5% CNTS + 40% SS316L

Spectra for the first and fifth layers of sample B and sample C are presented in Figs. 5(c)–(f). Spectra for the first and fifth layer of these FGM are very similar to the spectra for the first and fifth layers of sample A. 0.5% CNT was used in sample B and sample C, which is very

low quantity, therefore no peak is observed for CNT in the spectra for the first and fifth layers of these samples. From these XRD spectra, it is clearly shown that no phase transformation has occurred during sintering of these FGM.

3.6 Mechanical behaviour

3.6.1 Microhardness

The hardness of each layer of different FGM is measured by using microhardness tester. Microhardness indentation of each layer of FGM was carried out using a diamond indenter with a load of 1.96 N for 10 s. Loading conditions were kept similar for all samples to get consistency in the results. The hardness is resistance of materials to localized plastic deformation due to indentation. It is dependent on the percentage of densification, percentage of pores present at grain boundaries and in the grains, the presence of undesirable decomposed phases like tri-calcium phosphate and tetra-calcium phosphate and dispersion of the reinforced particles in the matrix.

In all FGM the first layer was made of HA (with 0.5% CNT in sample B and nano HA & 0.5% CNT in sample C) and in the subsequent layers, SS316L was added up to 40%. SS316L is ductile phase, therefore, its addition in brittle phase HA would lead to decrease in the hardness from top layer to the fifth layer of the FGM. The hardness for individual layers of different FGM (taken from average of 20 values of 2 or 3 samples) of each composition is shown in Fig. 6. As shown in Fig. 6, the hardness decreased for discrete layers of all FGM as the concentration of SS316L increased up to 40%. All FGM had the same trend for individual layers. In the case of sample A where only micro HA was used in the discrete layers, hardness values were found to be very low as compared to the other two FGM where CNT and nanocrystalline HA were used in sample B and sample C. Hardness obtained for the monolithic HA (i.e. HV 43.54), was very close to the value obtained by WANG and CHAKI [16]. Comparison of the first and fifth layers of sample A showed 23% decrease in the hardness value due to addition of 40%SS31L in the fifth layer of FGM. Similar trend in the hardness was found by CHU et al [19] who fabricated FGM of HA/Ti and found that hardness decreased as the concentration of Ti increased in the discrete layers of FGM.

The comparison between the hardness of the first layer of sample A and sample B, showed a valuable increase of 22% in the hardness due to addition of CNT in HA, which is in accordance to the results obtained by PIE et al [20] where they fabricated CNT reinforced HA composite coatings on the Ti substrate. These results are in support to the results obtained by densification (i.e. densification also increased with CNT addition). When

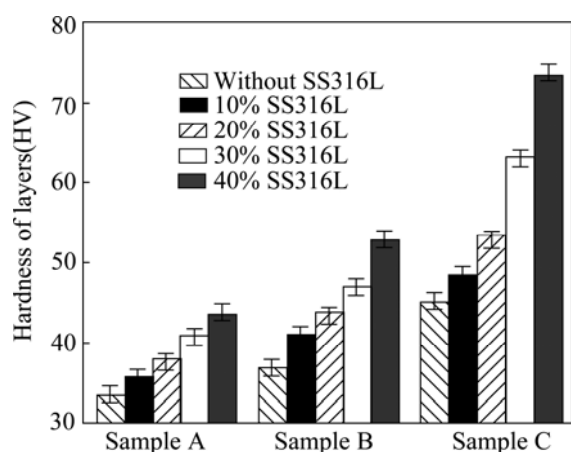


Fig. 6 Comparison of microhardness of various FGM layers

nanocrystalline HA was added to the sample C, hardness value increased again. This was due to the nanoparticles filling the pores and making it denser as compared to the sample A and sample B. The comparison of the first layer of sample A with sample C shows marginal increase of 65% hardness. The highest values of hardness of individual layers were obtained in the case of sample C in the present study.

3.6.2 Fracture toughness

Fracture toughness (K_{IC}) of the first and fifth layers of FGM was evaluated by indentation method by using the expression as given in Ref. [21]. In the present work, the tests were conducted at a load of 196 N for all samples with a loading duration of 10 s. Higher values of toughness for sample B and sample C were obtained as compared to sample A. The K_{IC} values for different layers of FGM were measured by indentation method are shown in the Fig. 7. From Fig. 7, it is clear that fracture toughness increases from the first layer to the fifth layer which is prime requirement of the FGM for knee implants. The K_{IC} value for monolithic HA layer is found to be $0.65 \text{ MPa}\cdot\text{m}^{1/2}$.

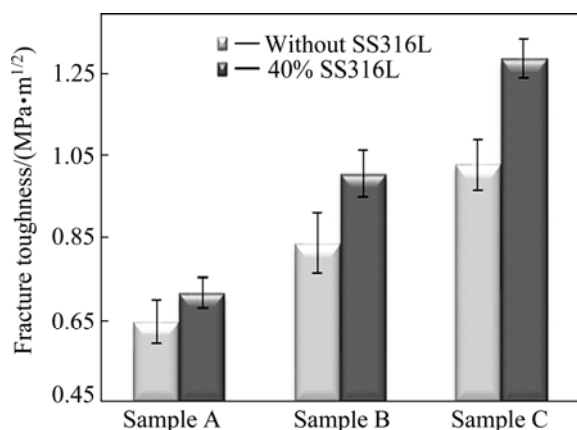


Fig. 7 Comparison of fracture toughness of first and fifth layers of different FGM measured by indentation method

HA showed values of $0.70 \text{ MPa}\cdot\text{m}^{1/2}$ [22], $0.68 \text{ MPa}\cdot\text{m}^{1/2}$ [23] and $0.75 \text{ MPa}\cdot\text{m}^{1/2}$ [24], when it was densified by SPS and HIP techniques respectively in the previous work. Value obtained in the present study is lower because pressureless sintering technique is used to densify the HA, but on the other hand, hardness value was very close to the results of previous work (i.e. HV 43.5). Considering K_{IC} values for the first and fifth layers of sample A, it shows clearly that the K_{IC} value increases from $0.65 \text{ MPa}\cdot\text{m}^{1/2}$ for monolithic micro HA to $0.72 \text{ MPa}\cdot\text{m}^{1/2}$ for micro HA + 40% SS316L (i.e. 23%). This increase in the toughness was due to reinforcement of HA matrix with the ductile particles of SS316L. The same behavior was obtained for other two FGM. The same trend for the toughness values of discrete layers of FGM was obtained by MISHINA et al [21]. They studied the FGM system of zirconia with SS316L and showed that with the addition of SS316L to zirconia improved the fracture toughness of the individual layers almost linearly.

For biomedical implants, sliding occurs on the surface of the ceramic HA in actual service conditions. Therefore, fracture toughness of HA layers of FGM is important. The fracture toughness of first layer of sample A (100%micro HA) is compared with sample B and sample C. It is found that the fracture toughness values of the first layer of sample B (micro HA + 0.5% CNT) and sample C ((50% micro/50% nano) HA + 0.5% CNT) are about 30% and 57% greater than that of monolithic HA layer of sample A. Hence, toughness is almost doubled in the case of sample C.

The comparison of the K_{IC} of layers of sample A with the sample B shows that addition of CNT in HA has improved its toughness and it is also explained by the previous studies [15,25]. Also in the case of sample C toughness was improved due to the presence of CNT and nanocrystalline HA, which bonds strongly with other particles in the FGM. Nanocrystalline HA has more surface area, and more surface energy, which resulted in the good densification, hardness and toughness of the sample C.

4 Conclusions

Functionally graded materials of three different compositions, sample A (micro HA+SS316L), sample B (micro HA + 0.5% CNT + SS316L) and sample C ((50% micro/50% nano) HA + 0.5% CNT + SS316L), were synthesized for biomedical implants successfully by the pressureless sintering technique. Densification of different layers of sample C is found to be higher as compared to sample A and sample B because nanocrystalline HA and CNT have been used with the

micron HA and SS316L in sample C. Hardness values of discrete layers decrease with increase of concentration of SS316L. It is HV 33.4 for layer having micro HA with 40% SS316L as compared to HV 44 for monolithic HA layer of sample A. Due to fine dispersion of CNT and addition of nanocrystalline HA, a marginal increase in the hardness is observed for all layers of sample B and sample C as compared to sample A. Fracture toughness is found to be increasing with increase of concentration of SS316L and it is $0.72 \text{ MPa}\cdot\text{m}^{1/2}$ for the fifth layer (micro HA + 40% SS316L) of sample A, compared with $0.65 \text{ MPa}\cdot\text{m}^{1/2}$ for monolithic HA layer. Fracture toughness is also increased to $0.84 \text{ MPa}\cdot\text{m}^{1/2}$ for the first layer of sample B (micro HA + 0.5% CNT) and $1.028 \text{ MPa}\cdot\text{m}^{1/2}$ for the first layer of sample C ((50% micro/50% nano) HA + 0.5% CNT).

Acknowledgements

The authors are thankful to GIK Institute for financial assistance and providing research facilities. This work is also supported by the Basic Research program through the National Research Foundation of Korea (NRF) funded by Ministry, Science and Technology (MEST) (2011-0030058)

References

- [1] METIKOŠ-HUKOVIĆ M, TKALČEC E, KWOKAL A, PILJAC J. An in vitro study of Ti and Ti-alloys coated with sol-gel derived hydroxyapatite coatings [J]. *Surface and Coatings Technology*, 2003, 165(1): 40–50.
- [2] SON J S, APPLEFORD M, ONG J L, WENKE J C, KIM J M, CHOI S H. Porous hydroxyapatite scaffold with three-dimensional localized drug delivery system using biodegradable microspheres [J]. *Journal of Controlled Release*, 2011, 153(2): 133–140.
- [3] SUCHANEK W, YOSHIMURA M. Processing and properties of hydroxyapatite-based biomaterials for use as hard tissue replacement implants [J]. *Journal of Materials Research*, 1998, 13(1): 94–117.
- [4] CHENG G J, PIRZADA D, CAI M, MOHANTY P, BANDYOPADHYAY A. Bioceramic coating of hydroxyapatite on titanium substrate with Nd-YAG laser [J]. *Materials Science and Engineering C*, 2005, 25(4): 541–547.
- [5] MIAO X, RUYS A J, MILTHORPE B K. Hydroxyapatite-316L fibre composites prepared by vibration assisted slip casting [J]. *Journal of Materials Science*, 2001, 36(13): 3323–3332.
- [6] RECLARU L, LERF R, ESCHLER P Y, MEYER J M. Corrosion behavior of a welded stainless-steel orthopedic implant [J]. *Biomaterials*, 2001, 22(3): 269–279.
- [7] SUMITA M, HANAWA T, TEOH S. Development of nitrogen-containing nickel-free austenitic stainless steels for metallic biomaterials-review [J]. *Materials Science and Engineering C*, 2004, 24(6–8): 753–760.
- [8] HAYNES D R, CROTTI T N, HAYWOOD M R. Corrosion of changes in biological effects of cobalt chrome alloy and 316L stainless steel prosthetic particles with age [J]. *Journal of Biomedical Materials Research*, 2000, 49(2): 167–175.
- [9] OH K T, KIM K N, LEE M, PARK Y S. Corrosion wear of high molybdenum and nitrogen stainless steel for biomedical applications [J]. *Journal of the Electrochemical Society*, 2002, 149(4): B146–B153.
- [10] SIVAKUMAR M, MUDALI U K, RAJESWARI S. In vitro electrochemical investigations of advanced stainless steels for applications as orthopaedic implants [J]. *Journal of Materials Engineering and Performance*, 1994, 3(6): 744–753.
- [11] SRIDHAR T. Sintering atmosphere and temperature effects on hydroxyapatite coated type 316L stainless steel [J]. *Corrosion Science*, 2003, 45(10): 2337–2359.
- [12] YANG C, WANG B, CHANG E, WU B. Bond degradation at the plasma-sprayed HA coating/Ti–6Al–4V alloy interface: An in vitro study [J]. *Journal of Materials Science: Materials in Medicine*, 1995, 6(5): 258–265.
- [13] ZENG H, LACEFIELD W R. XPS, EDX and FTIR analysis of pulsed laser deposited calcium phosphate bioceramic coatings: The effects of various process parameters [J]. *Biomaterials*, 2000, 21(1): 23–30.
- [14] XU J, KHOR K, SUI J, CHEN W. Preparation and characterization of a novel hydroxyapatite/carbon nanotubes composite and its interaction with osteoblast-like cells [J]. *Materials Science and Engineering C*, 2009, 29(1): 44–49.
- [15] BALANI K, ANDERSON R, LAHA T, ANDARA M, TERCERO J, CRUMPLER E. Plasma-sprayed carbon nanotube reinforced hydroxyapatite coatings and their interaction with human osteoblasts in vitro [J]. *Biomaterials*, 2007, 28(4): 618–624.
- [16] WANG P E, CHAKI T K. Sintering behaviour and mechanical properties of hydroxyapatite and dicalcium phosphate [J]. *Journal of Materials Science: Materials in Medicine*, 1993, 4(2): 150–158.
- [17] MURALITHRAN G, RAMESH S. The effects of sintering temperature on the properties of hydroxyapatite [J]. *Ceramics International*, 2000, 26(2): 221–230.
- [18] GERMAN R M. *Sintering theory and practice* [M]. New York: John Wiley & Sons, Inc., 1996: 181–184.
- [19] CHU Cheng-lin, ZHU Jing-chuan, YIN Zhong-da, WANG Shi-dong. Hydroxyapatite–Ti functionally graded biomaterial fabricated by powder metallurgy [J]. *Materials Science and Engineering A*, 1999, 271(1/2): 95–100.
- [20] PEI X, WANG J, WAN Q, KANG L, XIAO M, BAO H. Functionally graded carbon nanotubes/hydroxyapatite composite coating by laser cladding [J]. *Surface and Coatings Technology*, 2011, 205(19): 4380–4387.
- [21] MISHINA H, INUMARU Y, KAITOKU K. Fabrication of ZrO₂/AISi316L functionally graded materials for joint prostheses [J]. *Materials Science and Engineering A*, 2008, 475(1–2): 141–147.
- [22] S. KOBAYASHI W K, WAKAYAMA S. The effect of pressure during sintering on the strength and the fracture toughness of hydroxyapatite ceramics [J]. *Journal of Material Science: Material Medicine*, 2006, 17: 1089–1093.
- [23] LAU A K T, HUI D. The revolutionary creation of new advanced materials—carbon nanotube composites [J]. *Composites Part B: Engineering*, 2002, 33(4): 263–277.
- [24] AHMAD I, CAO H, CHEN H, ZHAO H, KENNEDY A, ZHU Y Q. Carbon nanotube toughened aluminium oxide nanocomposite [J]. *Journal of the European Ceramic Society*, 2010, 30(4): 865–873.
- [25] LI Hai-peng, ZHAO Nai-qin, LIU Yuan, LIANG Chun-yong, SHI Chun-sheng, DU Xi-wen, LI Jia-jun. Fabrication and properties of carbon nanotubes reinforced Fe/hydroxyapatite composites by in situ chemical vapor deposition [J]. *Composites A*, 2008, 39: 1128–1132.

生物植入用碳纳米管增强混合功能梯度材料的力学性能

M. Asif HUSSAIN¹, Adnan MAQBOOL^{1,2}, F. Ahmad KHALID¹, Nabi BAKHSH¹, Ali HUSSAIN²,
Jamil Ur RAHMAN², Jong Kyu PARK², Tae Gone PARK², Lee Jae HYUN², Myong Ho KIM²

1. Faculty of Materials Science and Engineering, GIK Institute of Engineering Sciences and Technology,
Topi, KPK, Pakistan;

2. Engineering Research Center for Integrated Mechatronics Materials and Components,
Changwon National University, Gyeongnam 641-773, Korea

摘要: 利用羟基磷灰石(HA)、不锈钢 316L(SS316L)和碳纳米管(CNT) 制备生物医学植入体用混合功能梯度材料(FGM)。加入 SS316L 和 CNT 增强功能梯度材料离散层的 HA 制成三种不同类型的功能梯度材料。第一种功能梯度材料加入 10%~40%(质量分数) 的 SS316L 强化微米 HA, 浓度梯度为 10%。第二种功能梯度材料, 在第一种功能梯度材料的基础上加入 0.5%(质量分数)的功能化碳纳米管。第三种功能梯度材料在第二种功能梯度材料的基础上加入微米 HA 和纳米 HA(1:1)的混合物。所有类型的功能梯度材料在相似的压缩参数和烧结参数下, 进行单轴压缩实验, 并采用无压烧结技术进行烧结。结果表明, 加入碳纳米管和纳米晶体 HA 提高了功能梯度材料的致密度。碳纳米管增强的功能梯度材料的硬度和断裂韧性增加, 但是微米和纳米晶体 HA 增强的功能梯度材料的硬度和断裂韧性的增加更明显。

关键词: 功能梯度材料; 羟基磷灰石; 纳米复合材料; 生物材料; 植入体

(Edited by Jun ZHAO)